A Comparative Study of Observed Northern Hemisphere Circulation Statistics Based on GFDL and NMC Analyses. Part II: Transient Eddy Statistics and the Energy Cycle

NGAR-CHEUNG LAU

Geophysical Fluid Dynamics Program, Princeton University, Princeton, NJ 08540

ABRAHAM H. OORT

Geophysical Fluid Dynamics Laboratory/NOAA, Princeton University, Princeton, NJ 08540

(Manuscript received 7 April 1981, in final form 29 November 1981)

ABSTRACT

The comparison between two sets of observed circulation statistics undertaken by Lau and Oort (1981) is continued in this study by examining the temporal variance and covariance statistics in these sets. The first (GFDL) set is compiled by interpolating monthly averaged station statistics. The second set is based on twice-daily operational NMC analyses. The statistics for six winter and six summer seasons within the 1966–73 period are compared. The hemispheric fields examined include transient eddy kinetic energy at 300 mb, root-mean-squares of geopotential height and temperature at 300 and 850 mb, respectively, the horizontal transport by transient eddies of westerly momentum and geopotential height at 300 mb, and of heat at 850 mb. The patterns of horizontal eddy transports are presented in a vectorial format to delineate local relationships with the time-mean flow and the centers of eddy activity. Latitude–height distributions for zonally-averaged patterns of the above statistics are also presented.

The transient eddy statistics in the two sets are in good agreement over regions with adequate data coverage. The NMC set generally gives relatively higher eddy amplitudes and stronger eddy transports over the data-sparse oceans. The maximum deviations between the two sets in these regions are about 20–30%.

The two sets of analyses are further used to calculate the spatial integrals for the energy reservoirs and various energy conversion rates in the atmosphere. The transient and stationary eddies are treated separately in the formulation of the energy cycle. The largest differences are found in the transfer rate of kinetic energy from the stationary waves to the transient disturbances, and for the terms associated with the conversion of available potential energy into kinetic energy. The GFDL and NMC estimates of the other components of the energy cycle do not differ from each other by >20%. The results from both sets of analyses imply that the transient eddies are very efficient in depleting the available potential energy of the stationary waves through their ability to transport heat down the local temperature gradient. The dissipative time scale associated with this mechanism is several days.

1. Introduction

In Part I of this study (Lau and Oort, 1981; hereafter referred to as I), the observed time-mean atmospheric fields from two sets of circulation statistics were compared. These sets of analyses are the products of two fundamentally different handling procedures. The set compiled at the Geophysical Fluid Dynamics Laboratory (GFDL analyses) is composed of horizontal objective analyses of monthly mean statistics accumulated at individual rawinsonde stations. The second set made use of gridded values for twice-daily synoptic charts produced by the operational forecast-analysis cycles at the National Meteorological Center (NMC analyses). It was noted in I that the time-mean statistics in the two sets are in good agreement over regions covered by a dense rawinsonde network. On the other hand, systematic differences between the two sets were found over the data-sparse areas. (The distribution of reporting rawinsonde stations in the early 1970's is illustrated in Fig. 1 of I.) The reader is referred to I for a detailed description of the nature of these similarities and differences, and of the data handling procedures for the GFDL and NMC sets. Earlier studies on this subject by other investigators and the motivation for undertaking the present comparative study were also discussed in I.

In this part of the study, we extend the findings in I by examining the transient eddy variance and covariance statistics in the two sets of analyses, and by comparing the integrals for some of the important components in the atmospheric energy cycle.

The data base for this part of the study is described in Section 2. The differences between the hemispheric distributions of transient eddy variance statistics in the two sets are presented in Section 3. Variations with height of the local differences are

0027-0644/82/080889-18$08.50

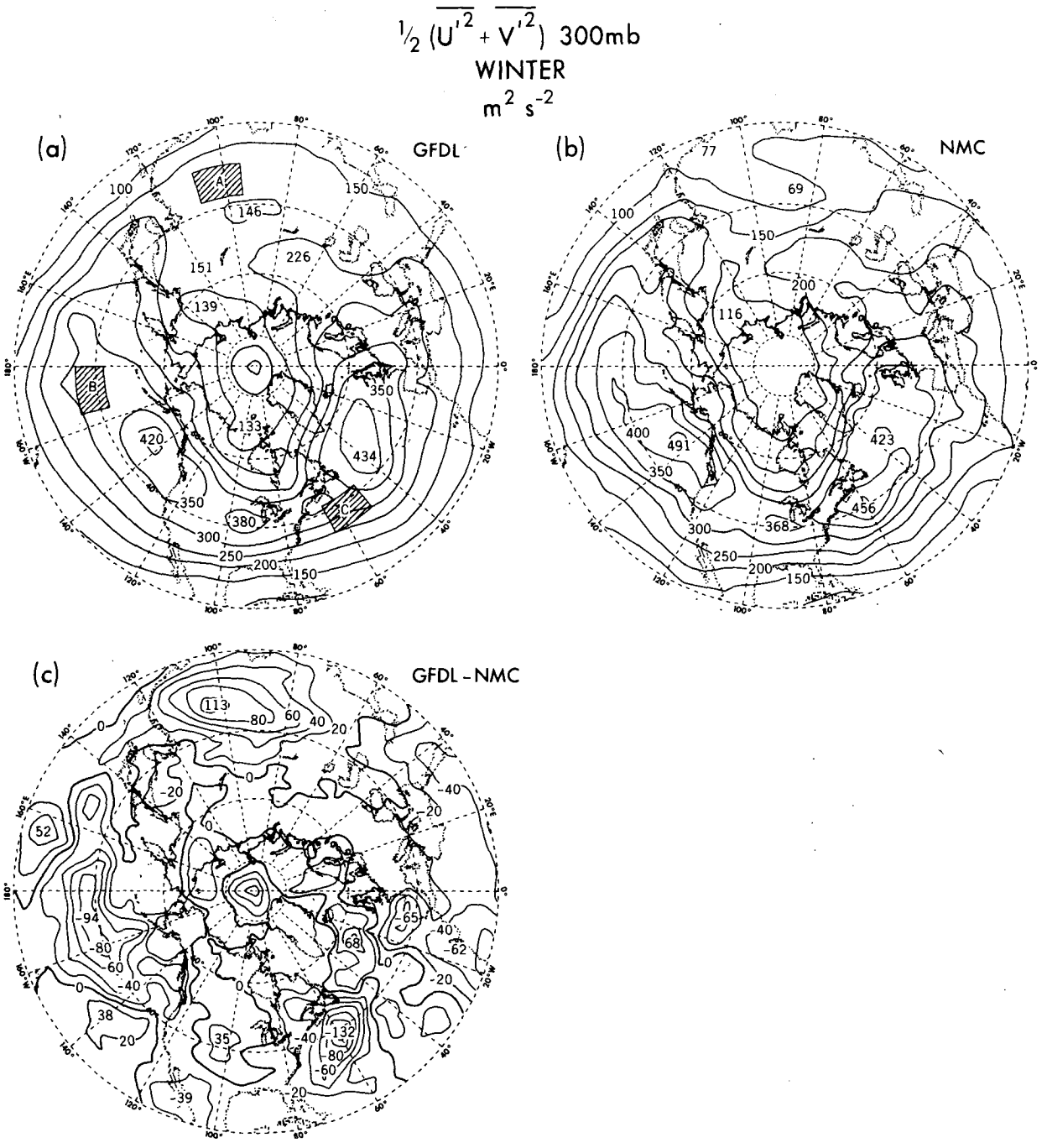

FIG. 1. Wintertime distributions of transient eddy kinetic energy ($m^2 s^{-2}$) at 300 mb, based on (a) GFDL analysis and (b) NMC analysis. The difference map (c) shows the pattern obtained by subtracting the NMC analysis from the GFDL analysis. The shaded patches in (a) indicate those regions for which vertical profiles of the differences between the GFDL and NMC analyses will be presented.

depicted by vertical profiles. The horizontal transports of westerly momentum, sensible heat and geopotential height by transient eddies are presented in Section 4 in a vectorial format, so that the differences in amplitude and orientation of the flux vectors in the two sets can be easily examined. Latitude–height distributions of the zonally averaged transient eddy variance and covariance statistics are then compared in Section 5. Finally, the implications of the differences between the GFDL and NMC sets on the nature of the atmospheric energy cycle are explored in Section 6.

2. Data sets and analysis procedures

The data base for this portion of the study is slightly different from that used in I. It consists of selected statistics from the GFDL and NMC analyses for the six winter seasons from 1966/67 to 1972/73 (except 1969/70, for which the NMC wind analyses are mostly missing), and the six summer seasons from 1967 to 1972. Further technical details of the GFDL and NMC sets may be found in Oort (1982) and Lau *et al.* (1981), respectively.

The winter season for the GFDL set is taken to be the 90-day period from 1 December to 28 February, while for the NMC set the winter season corresponds to the 120 day period from 15 November to 14 March (13 March in leap years). The transient eddy statistics were first computed for each individual winter, and were then averaged over the six winters. The transient fluctuations hence represent departures of the daily values within a given winter from the seasonal mean for that particular winter.

A different "wintertime" set of GFDL statistics consisting of weighted averages of monthly statistics for November, December, January, February and March was also compared with the NMC set as defined above. On the basis of this and other experiments, we conclude that the difference in the definition of the winter season does not explain the discrepancies between the two sets of analyses shown in the following sections.

For the summer season, the NMC statistics were compiled by G. H. White of the University of Washington using data for the 120-day period from 1 June to 30 September. The processing of the NMC analyses in this season was somewhat different from the procedures for the winter data. The former involved the additional step of removing the seasonal cycle by subtracting a parabola from the time series. The parabola was obtained by the method of least-squares, and was determined individually for each grid point in each summer. In order to also minimize the contribution of the seasonal cycle to the summer transient eddy statistics in the GFDL analyses, the summertime GFDL statistics were computed by averaging the monthly transient eddy statistics for June, July, August and September. Thus, in contrast to the winter season, the transient fluctuations in the summer season represent departures of the data values within a given summer month from the corresponding monthly mean.

3. Hemispheric distributions of temporal variance fields

a. Winter season

1) KINETIC ENERGY

In Fig. 1 are shown the distributions of transient eddy kinetic energy $\frac{1}{2}(\overline{u'^2} + \overline{v'^2})$ at 300 mb, based on a) GFDL and b) NMC analyses. Here the overbar denotes a time average and the prime a deviation from this time average. The difference between these two fields is displayed in Fig. 1c. There is good agreement between the two data sets over most of the land areas. A notable exception is the southeastern portion of the Asian continent, where the GFDL set gives relatively higher eddy kinetic energy. The differences between the two sets are large over the data-sparse oceans. The transient eddy kinetic energy in the NMC set is seen to be relatively higher over the central Pacific and western Atlantic. The vertical profiles in Fig. 2 illustrate the variation with height of the differences noted above. These profiles were obtained by averaging the differences over the 15° (longitude) × 7.5° (latitude) patches shown in Fig. 1a. The location of each patch corresponds to a site of large discrepancy between the two sets (see Fig. 1c). The shaded envelopes in Fig. 2 correspond to the extent of ±1 standard deviation of the differences

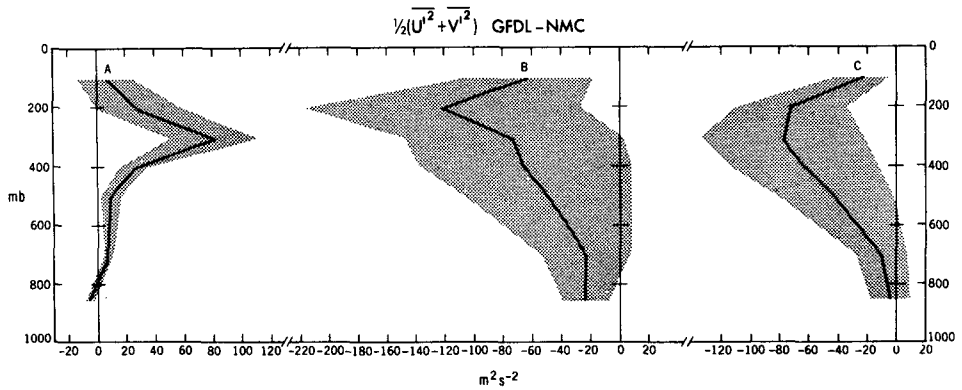

FIG. 2. Vertical profiles of the differences in transient eddy kinetic energy ($m^2 s^{-2}$) between the two analyses (GFDL minus NMC) averaged over the individual patches shown in Fig. 1a. The shading indicates the extent of ±1 standard deviation of the differences between the two data sets for the six individual winter seasons.

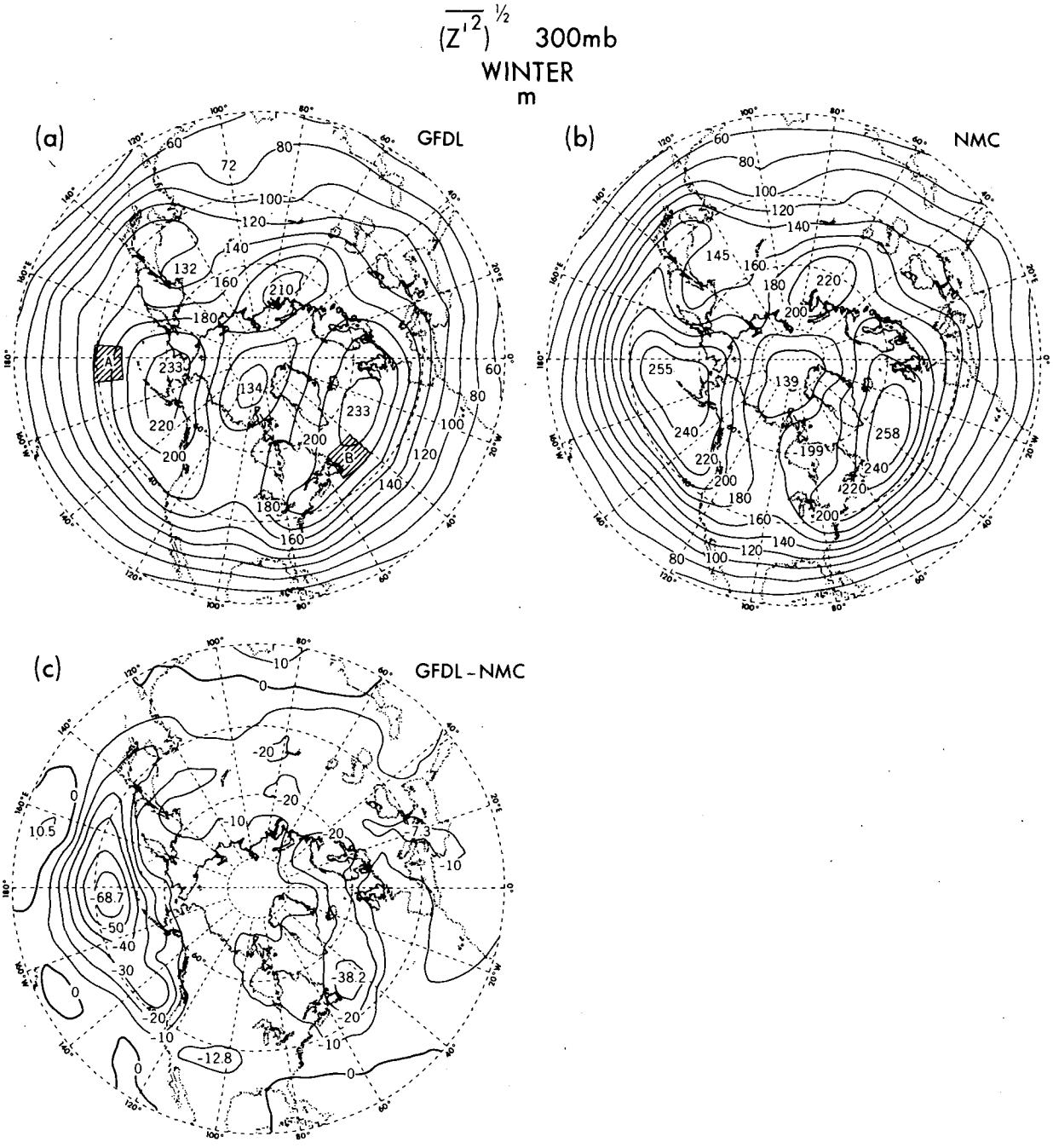

FIG. 3. As in Fig. 1, but for root-mean-square of geopotential height (m) at 300 mb.

between the GFDL and NMC analyses for six individual winter seasons. The profiles indicate that the differences between the two sets tend to be of the same sign throughout the atmospheric column between 700 and 100 mb, with maxima near the tropopause level.

2) GEOPOTENTIAL HEIGHT FLUCTUATIONS

The distributions of the root-mean-square (rms) of geopotential height $(\overline{z'^2})^{1/2}$ at 300 mb are compared in Fig. 3. The two sets exhibit a good correspondence over those regions which are covered by a dense rawinsonde network (see Fig. 1 in I). The largest differences occur over the central Pacific and western Atlantic, where the amplitude of the geopotential height fluctuations in the NMC set is stronger by as much as 60 m. The vertical profiles of the differences over the patches located in these two regions (see Fig. 3a) are shown in Fig. 4. The difference between the two sets of analyses attains a maximum value at the 200 mb level.

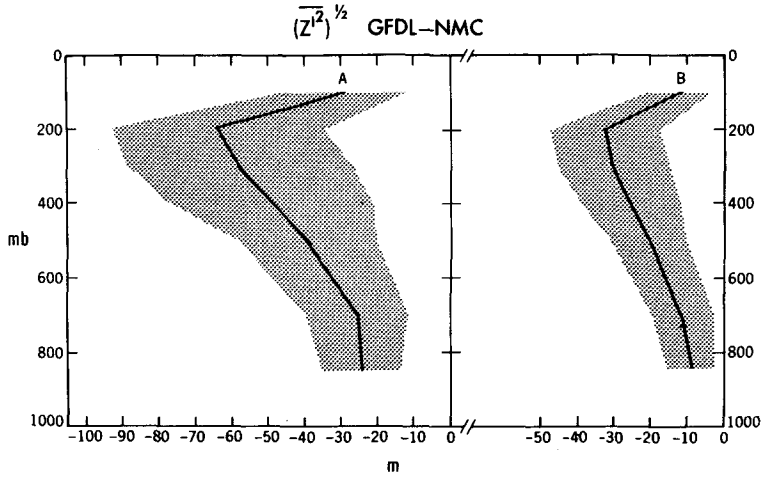

FIG. 4. As in Fig. 2, but for root-mean-square of geopotential height (m) averaged over the individual patches shown in Fig. 3a.

3) TEMPERATURE FLUCTUATIONS

The GFDL and NMC patterns of the rms of temperature $(\overline{T'^2})^{1/2}$ at 850 mb are displayed in Figs. 5a and 5b. The differences between the two sets (Fig. 5c) are also largest over the ocean basins, where the GFDL set gives relatively weaker temperature fluctuations. The vertical profiles of these differences (Fig. 6) indicate that the amplitude of the deviations is fairly uniform with height in the lower and middle troposphere.

b. Summer season

The differences between the summertime analyses in the GFDL and NMC sets are presented in Fig. 7, for a) transient eddy kinetic energy at 300 mb, b) rms geopotential height at 300 mb, and c) rms temperature at 850 mb. It should be noted that the different methods for removing the seasonal cycle in the two sets (see Section 2) may partially account for some of the features in this figure.

On the whole, most of the major features noted in the winter season (Figs. 1c, 3c and 5c) are also identifiable in the corresponding maps for summer. In particular, the patterns in Fig. 7 indicate that the NMC set yields stronger eddy activities for all three parameters along an elongated region over the central Pacific Ocean at ~45°N. A new feature in summer is the relatively stronger transient fluctuation in the GFDL sets over the eastern Pacific between 20° and 40°N.

4. Hemispheric distributions of horizontal transports by transient eddies

In this section the transport properties of the transient disturbances during the winter season are depicted by vectors. This method of presentation was used by Lau and Wallace (1979) for examining the eddy transports in relation to the local time-mean flow and the centers of eddy activity. The horizontal eddy transport of a quantity x over a given grid point

$$\mathbf{F}(x) \equiv \overline{u'x'}\,\mathbf{i} + \overline{v'x'}\,\mathbf{j}$$

is represented by an arrow centered over that grid point. The magnitude and direction of the local eddy transport are given by the length and orientation of the arrow, respectively. Here **i** and **j** denote the unit vectors in the zonal and meridional directions, respectively. In this section we shall examine the differences between the temporal covariance statistics in the two sets by comparing the local eddy flux vectors.

a. Momentum transport

The horizontal transport of westerly momentum by the transient disturbances $\mathbf{F}(u)$ at 300 mb is shown in Fig. 8 for a) GFDL and b) NMC analyses. Superimposed on this pattern are contours depicting the time averaged zonal wind $\bar{u}$ at 300 mb for the corresponding data set. The contours in Fig. 8c represent the differences in local magnitude of the momentum flux vectors in the two sets. The regions with significant discrepancies in the orientation of the flux vectors are indicated by shading in the same figure. It is evident from Figs. 8a and 8b that $\mathbf{F}(u)$ is dominated by the zonal flux component, i.e., $|\overline{u'u'}| \gg |\overline{v'u'}|$. By decomposing the NMC analyses for $\mathbf{F}(u)$ into nondivergent and irrotational parts, Lau and Wallace (1979, Fig. 9a) have noted that the eddy fluxes of westerly momentum tend to converge over western North America and western Europe, where the time-averaged zonal flow is relatively weak. Conversely, they tend to diverge over eastern Asia, where the stationary flow is relatively strong. These features are still discernible in the NMC pattern (Fig. 8b) presented here. The flux vectors in the GFDL pattern (Fig. 8a) exhibit less variation with longitude, and such relationships between momen-

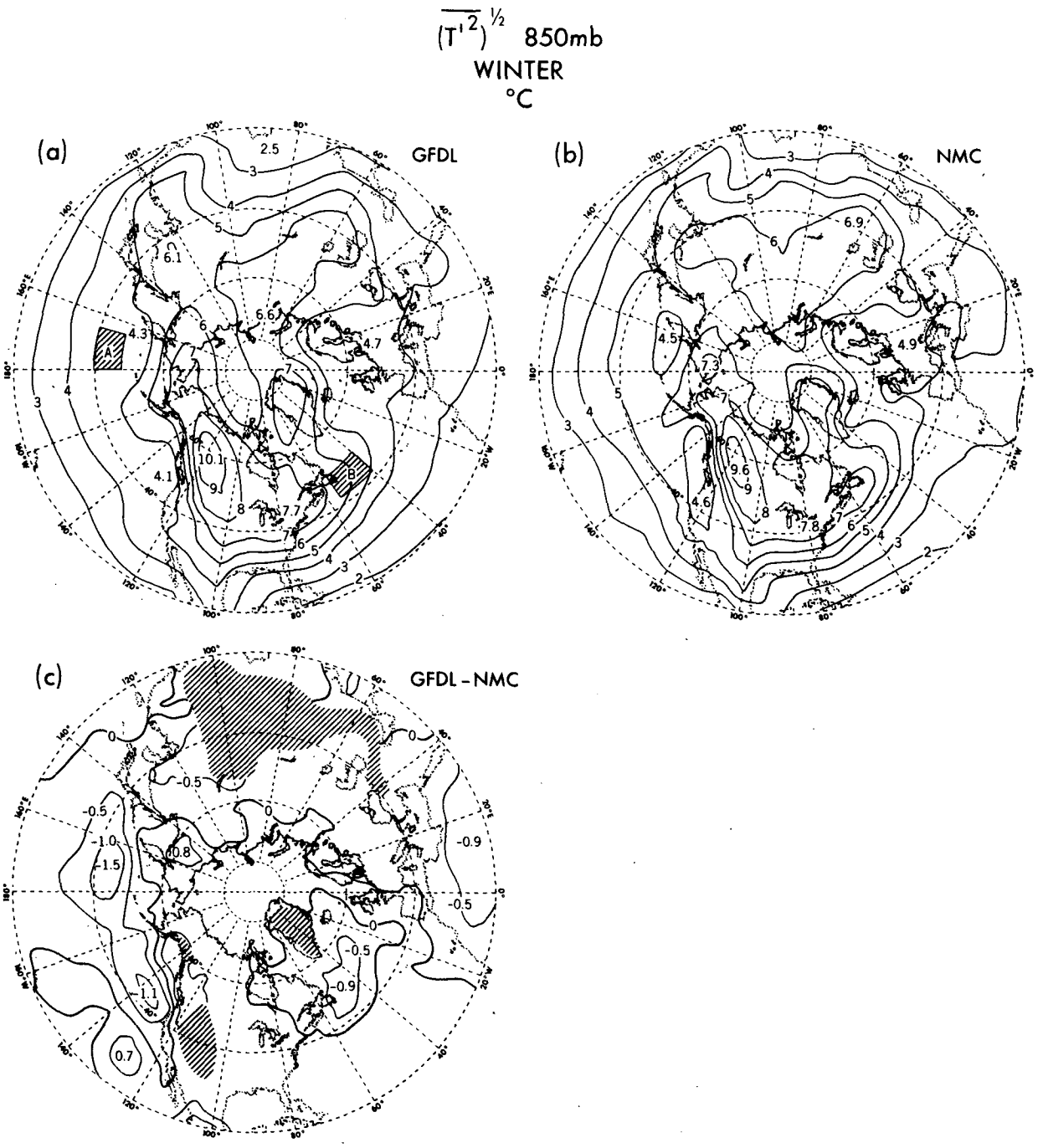

FIG. 5. As in Fig. 1, but for root-mean-square of temperature (°C) at 850 mb. The hatched areas in (c) indicate local topographic heights greater than 1500 m.

tum transports and the time-mean flow are less evident. Fig. 8c indicates that the eddy momentum transports in the GFDL set are relatively weaker over the oceans, and relatively stronger over southeastern Asia. These regions, together with northern Africa, are also characterized by significant discrepancies in the orientation of the momentum flux vectors.

b. Geopotential height transport

The vectors for the transport of geopotential height by transient eddies $\mathbf{F}(z)$ at 300 mb are displayed in Fig. 9, for a) GFDL and b) NMC analyses. The contours in these maps represent the isolines of the temporal variance of geopotential height $\overline{z'^2}$ at 300

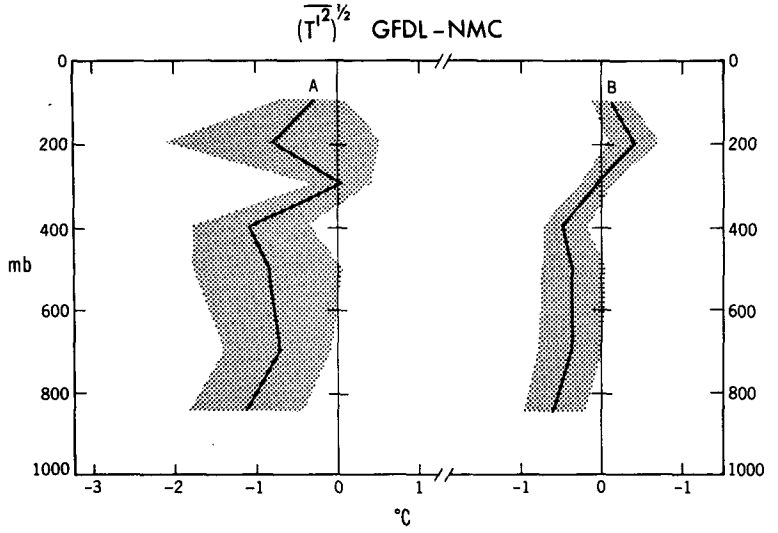

FIG. 6. As in Fig. 2, but for root-mean-square of temperature (°C) averaged over the individual patches shown in Fig. 5a.

mb. The differences between the two sets in the magnitude and orientation of the flux vectors are indicated in Fig. 9c by contours and shading, respectively. Lau and Wallace (1979) have pointed out that, for quasi-geostrophic motion,

$$\mathbf{F}(z) \approx \frac{g}{2f}\,\mathbf{k} \times \nabla \overline{z'^2}. \tag{1}$$

Here $\mathbf{k}$ is the vertical unit vector, g the gravitational acceleration, and f the Coriolis parameter. Thus, one would expect the flux vectors in the $\mathbf{F}(z)$ field to be aligned with the contours of $\overline{z'^2}$, and to circulate around centers of maximum geopotential height fluctuation in a clockwise fashion, and *vice versa*. Moreover, the magnitude of these flux vectors should be proportional to the absolute value of the horizontal gradient of the $\overline{z'^2}$ field. These relationships show up clearly in the NMC pattern (Fig. 9b) for the entire hemispheric domain. The GFDL pattern (Fig. 9a) also suggests that the vector flux of geopotential energy is closely related to the contours of $\overline{z'^2}$. However, the magnitude of the arrows in the GFDL pattern over the oceans is too small to be consistent with the strong gradients of the $\overline{z'^2}$ contours in those regions. Fig. 9c shows more explicitly the differences between the two sets of analyses over the oceans.

c. *Heat transport*

Figs. 10a and 10b show the horizontal heat transports by the transient eddies at 850 mb as given by the two sets of analyses. The time-averaged temperature distributions at the same level are also shown. The eddy heat flux data from the two sets are compared in Fig. 10c, using a similar display technique as those used in Figs. 8c and 9c. It is evident that the heat flux vectors in both sets exhibit a distinct tendency to be directed towards lower temperature. The eddy heat transports converge over northeastern Canada and eastern Siberia, which are colder than other regions in the same zonal belt. Conversely, these transports diverge over the relatively warm oceans. Both sets of analyses imply that the transient disturbances tend to destroy the departures from zonal symmetry of the time-mean temperature field (see Lau, 1979). The largest differences between the two sets are again found over the oceans (Fig. 10c), where the magnitude of the heat fluxes in the GFDL set is smaller.

5. Latitude–height distributions of zonally averaged transient eddy statistics

a. *Temporal variance statistics*

Fig. 11 shows the latitude–height distributions of the zonal means of a) transient eddy kinetic energy, b) rms geopotential height and c) rms temperature, for GFDL analyses (left panel), NMC analyses (middle panel), and the difference between the two sets (right panel). It is seen that the two sets give qualitatively similar patterns for these statistics. The weaker transient fluctuations in the GFDL analyses over the maritime areas lead to relatively lower estimates of the zonally averaged quantities. Maximum differences are ~10–20%.

b. *Temporal covariance statistics*

The zonally averaged wintertime distributions of the poleward transport of a) westerly momentum, b) geopotential height and c) heat by the transient ed-

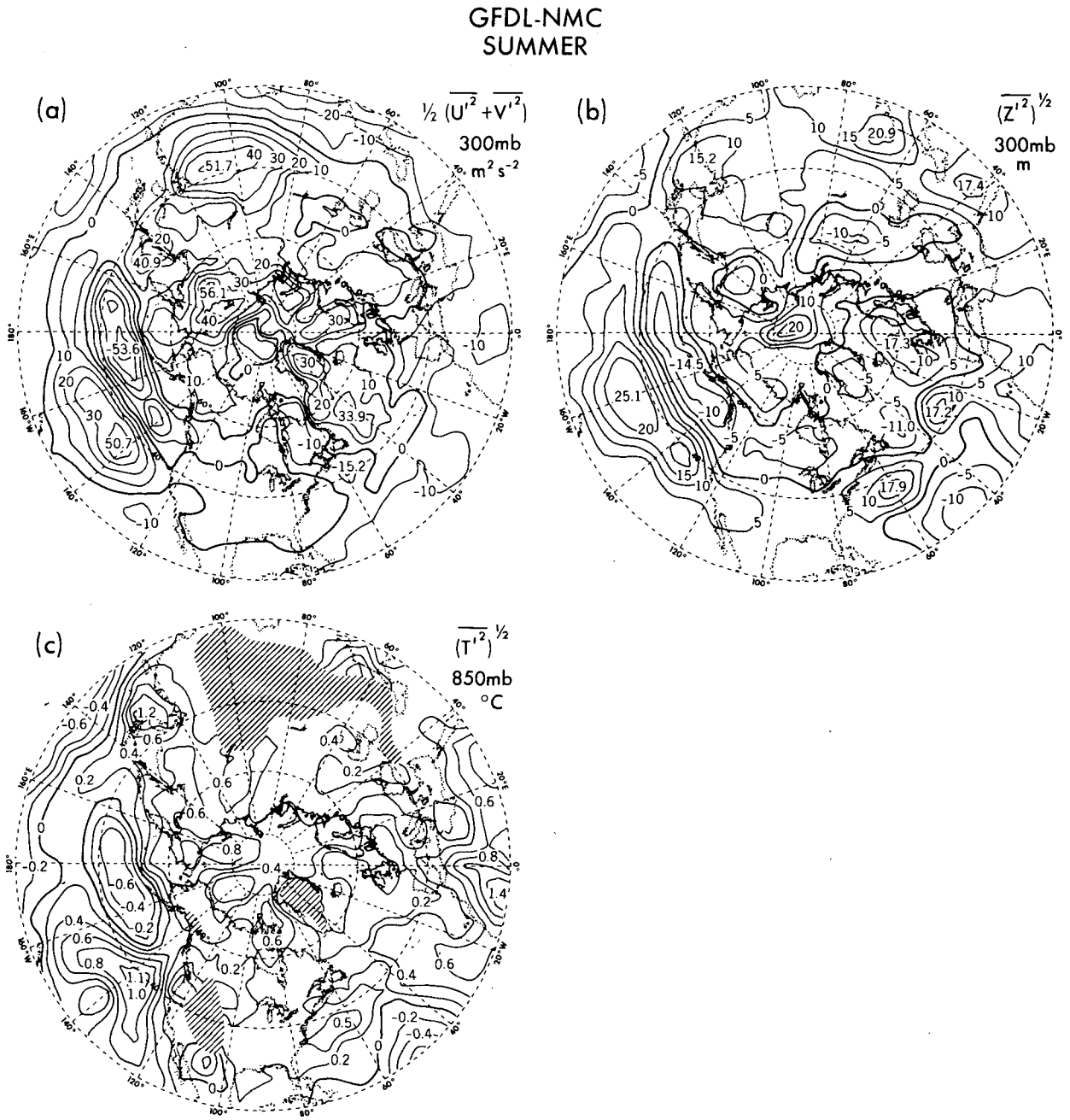

FIG. 7. Difference maps obtained by subtracting the NMC analysis from the corresponding GFDL analysis, based on the six-summer averages of (a) transient eddy kinetic energy ($m^2 s^{-2}$) at 300 mb, (b) root-mean-square of geopotential height (m) at 300 mb, and (c) root-mean-square of temperature (°C) at 850 mb (hatched areas indicate local topographic heights greater than 1500 m).

dies are compared in Fig. 12. The amplitude of the poleward momentum flux near the subtropical tropopause in the GFDL pattern is approximately 70–80% of the corresponding value in the NMC pattern (Fig. 12a). On the other hand, the equatorward transport of geopotential height in the GFDL pattern is stronger by a factor of ~1.5 (Fig. 12b). There is a good correspondence between the GFDL and NMC patterns for eddy heat transport (Fig. 12c). The GFDL set gives slightly weaker heat fluxes in the troposphere.

Rosen and Salstein (1980, Figs. 10 and 13) have also compared two similar sets of zonally averaged statistics on momentum and heat transports by transient eddies. These sets of analyses were compiled from objective analyses of station data and from op-

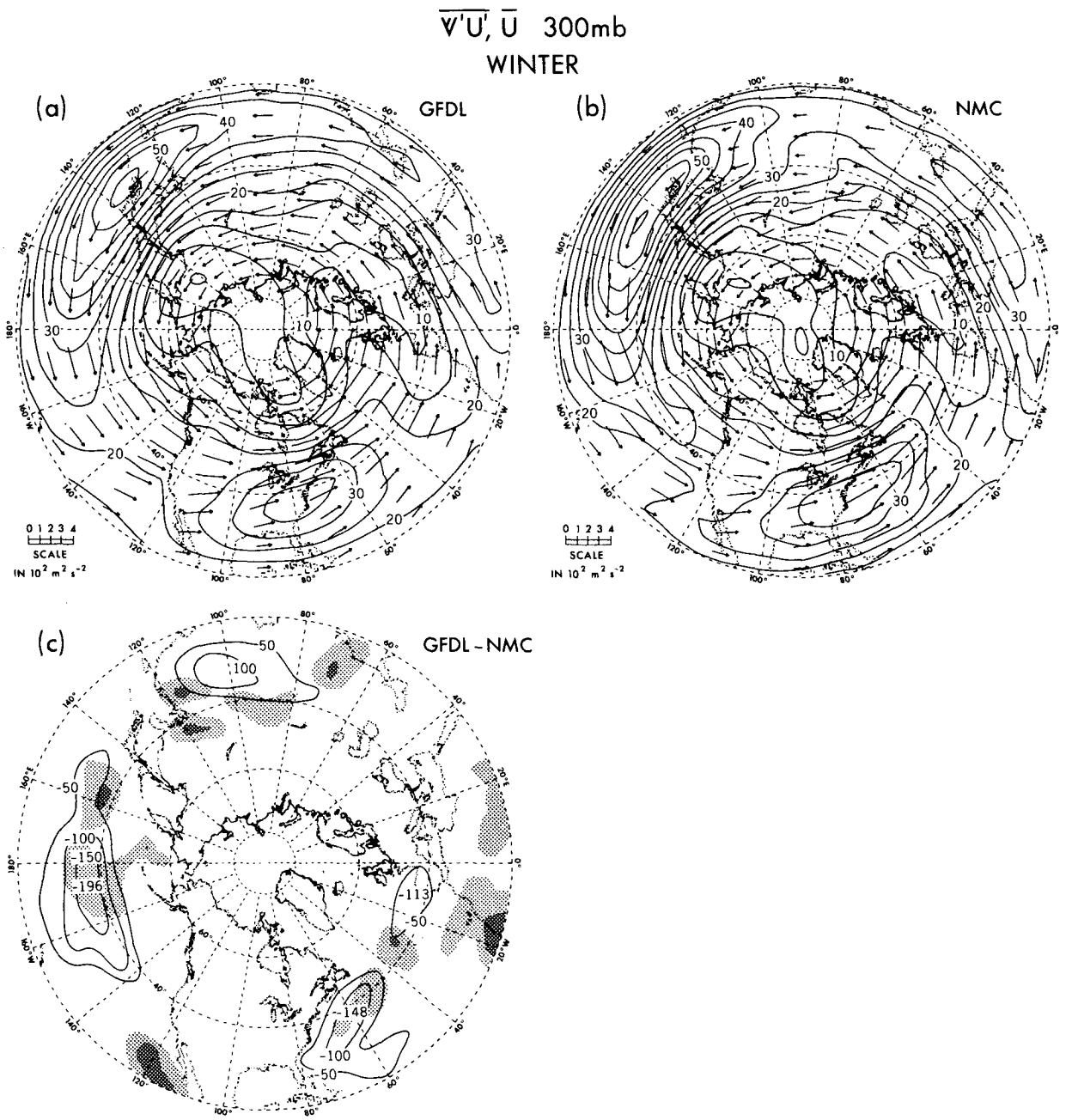

FIG. 8. Wintertime distributions of the horizontal transport of westerly momentum by transient eddies (vectors; $m^2\ s^{-2}$) and time-averaged zonal wind (contours; $m\ s^{-1}$) at 300 mb, based on (a) GFDL analysis and (b) NMC analysis. The length scale for the vectors is given in the lower left-hand corner of each map. Arrows too short to show up clearly have been omitted. The contours in (c) show the difference between the magnitude of the horizontal eddy momentum flux vectors in the two analyses (GFDL minus NMC; $m^2\ s^{-2}$). The zero-contour is not plotted for the sake of clarity. The light (heavy) shading in (c) indicates regions where the orientation of the eddy momentum flux vectors in the two analyses differ by more than 5° (10°).

erational NMC Hough analyses for the winter of 1976–77. They noted that the two analyses yield qualitatively similar patterns. Contrary to the results presented here, the intensity of the eddy fluxes given by the NMC analyses is comparatively weaker in their study.

6. Estimation of the atmospheric energy cycle

The atmospheric energy cycle as formulated first by Lorenz (1955) is a convenient framework for describing some of the integrated effects of the differences between the two sets of analyses noted here

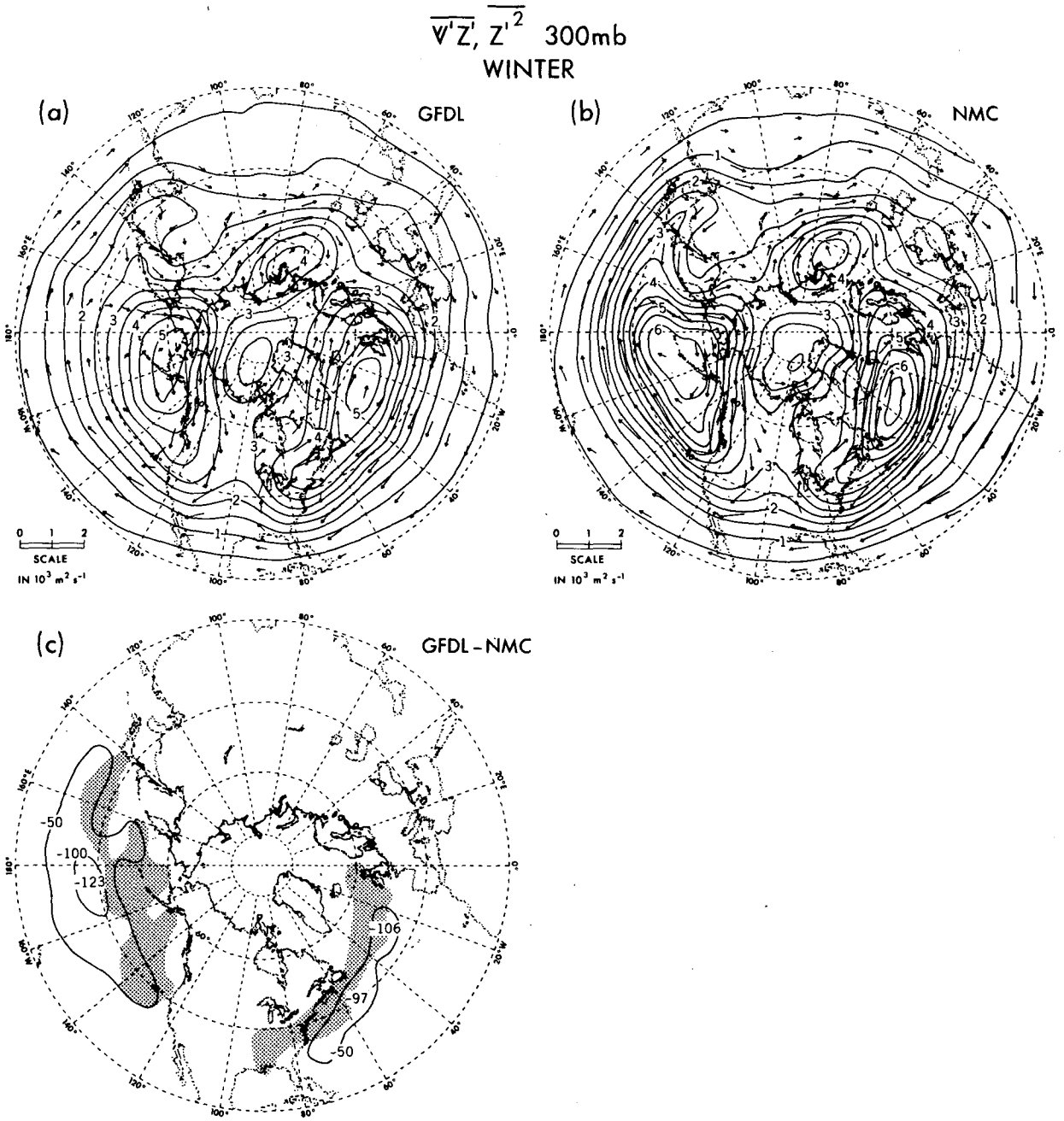

FIG. 9. As in Fig. 8, but for eddy transport of geopotential height (vectors; $m^2\ s^{-1}$) and temporal variance of geopotential height (contours; $10^4\ m^2$) at 300 mb. The shading in (c) indicates regions where the orientation of the eddy geopotential flux vectors in the two analyses differ by more than 20°.

and in I. We shall use the specific formulation given in Peixóto and Oort (1974, hereafter referred to as PO) to define the integrals for the various forms of atmospheric energy and for the energy conversion processes. The reader is referred to that paper for pertinent details. A novel feature in the present study is the partitioning of the eddies (i.e., those quantities in PO with subscripts E) into contributions from standing and transient eddies, which will be denoted by subscripts SE and TE, respectively. In doing so, the interactive processes between the zonal mean flow, the stationary waves and the transient disturbances can be explicitly evaluated. A similar decomposition of the eddies has been used by Holopainen (1970) to study the energy balance of the stationary waves. The expressions for various components of the energy cycle are given in the Appendix. The integrals are computed using the wintertime statistics in the

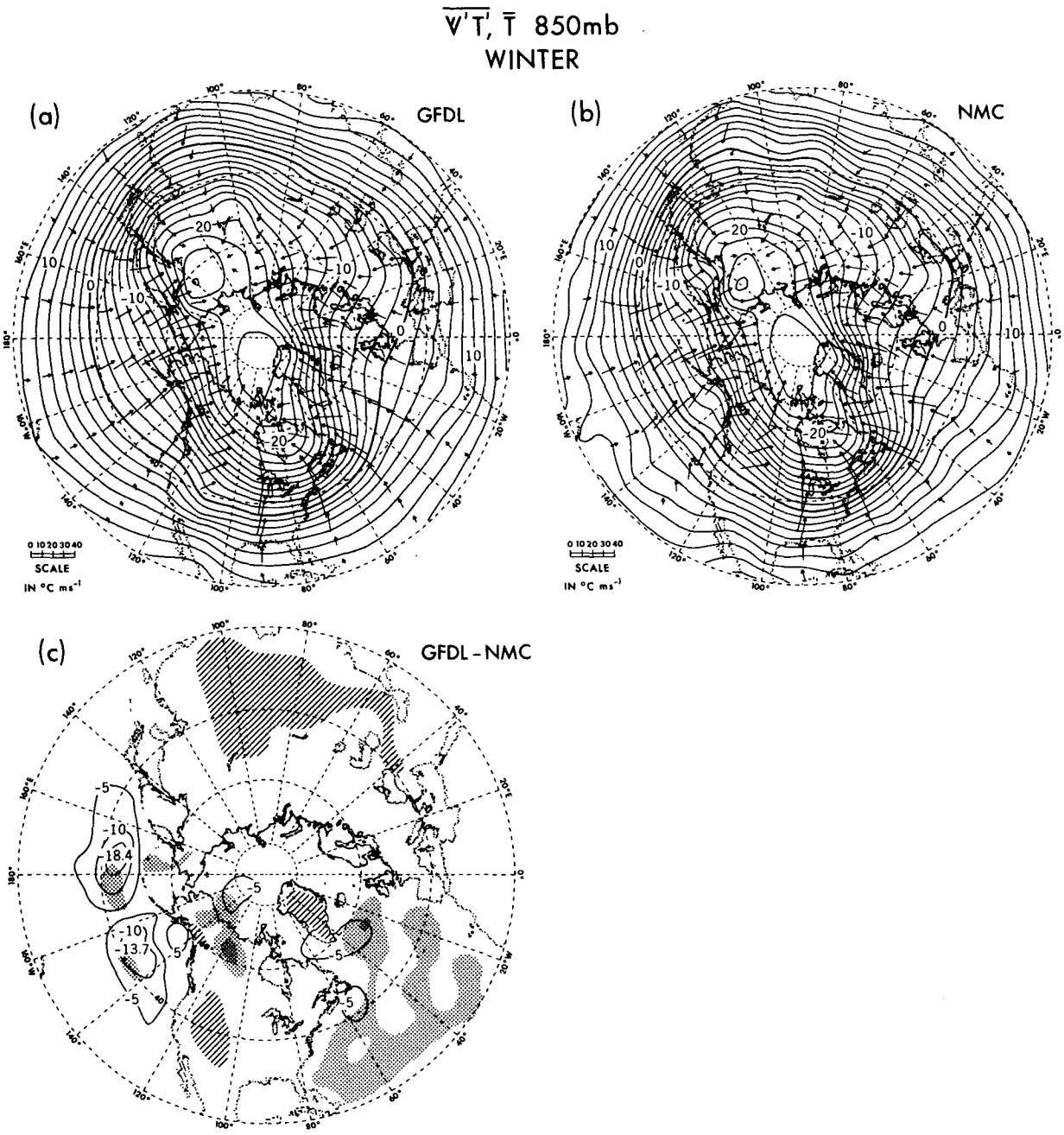

FIG. 10. As in Fig. 8, but for eddy transport of heat (vectors; °C m s^{-1}) and time-averaged temperature (contours; °C) at 850 mb. The light (heavy) shading in (c) indicates regions where the orientation of the eddy heat flux vectors in the two analyses differ by more than 10° (20°). The hatched areas in (c) correspond to topographic heights greater than 1500 m.

GFDL and NMC data sets for a domain extending in the horizontal direction from the 20°N latitude circle to the North Pole, and in the vertical from 850 to 100 mb. In this study we shall confine our attention to those terms in the energy balance which can be evaluated directly from the available data. A comprehensive picture of the full cycle is not attempted here.

The box diagrams in Fig. 13 show the estimates of various terms in the energy cycle using a) GFDL and b) NMC analyses. The following similarities and differences between the two sets are evident:

• The estimates of the various forms of atmospheric energy (i.e., K_M, K_{TE}, P_M, P_{SE} and P_{TE}) are generally in good agreement. The standing eddy kinetic energy K_{SE} as given by the GFDL analyses is ~80% of the corresponding NMC value. This is pri-

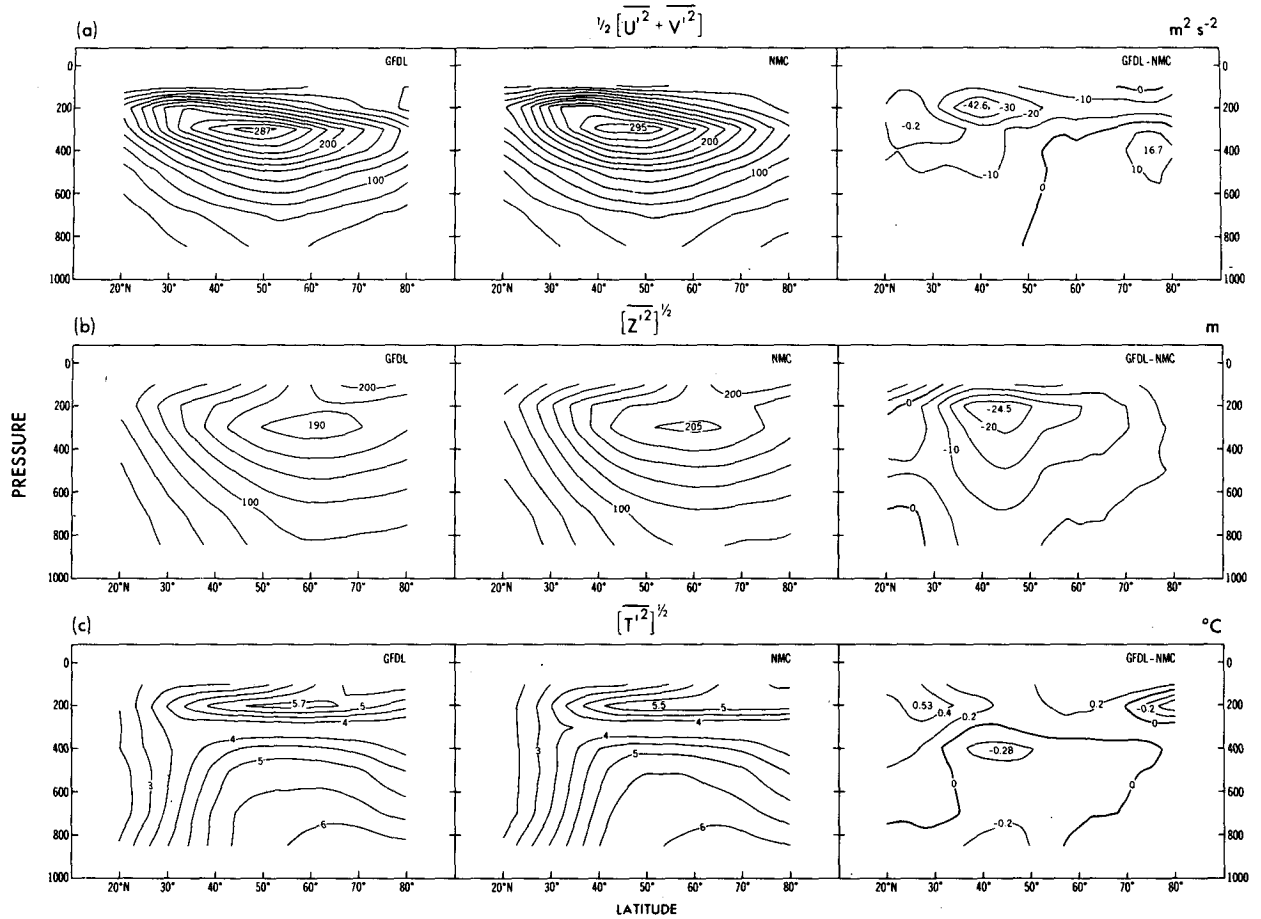

FIG. 11. Latitude–height sections of the zonal mean of (a) transient eddy kinetic energy ($m^2\ s^{-2}$), (b) root-mean-square of geopotential height (m), and (c) root-mean-square of temperature (°C), based on GFDL analysis (left panel) and NMC analysis (middle panel) for the winter season. The differences between the two sets (GFDL minus NMC) are shown in the right panel.

marily a result of the relatively weaker time averaged zonal flow over the data-sparse oceans in the GFDL set (see Figs. 3 and 14a in I).

- The poleward heat transports by the standing and transient eddies tend to extract available potential energy from the zonal mean flow, i.e., $C(P_M, P_{SE}) > 0$, $C(P_M, P_{TE}) > 0$. Since the GFDL analyses generally give weaker heat fluxes (see Fig. 15c in I and Fig. 12c in this paper), the GFDL estimates of the intensity of these conversion processes are lower by ~20%.

- Both sets of analyses indicate a conversion of kinetic energy from the eddies to the zonally averaged circulation, i.e., $C(K_{SE}, K_M) > 0$, $C(K_{TE}, K_M) > 0$. The two sets also give similar estimates of the intensity of these transformation processes.

- The transient disturbances are efficient in draining available potential energy from the stationary waves, i.e., $C(P_{SE}, P_{TE}) > 0$. This results from the tendency for these disturbances to transport heat down the local time-averaged temperature gradient (see Fig. 10). The estimate of this term using the GFDL set is ~70% of that using the NMC set.

- The estimates of $C(K_{SE}, K_{TE})$ given by the two data sets are quite different. This discrepancy should be viewed in light of the following considerations. The principal terms in the expression for $C(K_{SE}, K_{TE})$ are $-(\overline{u'u'}^*/a\ \cos\phi)(\partial\bar{u}^*/\partial\lambda)$ and $-(\overline{v'v'}^*/a)(\partial\bar{v}^*/\partial\phi)$ (see Appendix). It is seen from Fig. 8 that $-(\overline{u'u'}^*/a\ \cos\phi)(\partial\bar{u}^*/\partial\lambda)$ is positive between 20 and 45°N, and negative poleward of 50°N. Similarly, examination of the patterns of $\overline{v'v'}$ (which resemble those shown in Fig. 1) and $\bar{v}$ (see Fig. 5 of I) indicate that $-(\overline{v'v'}^*/a)(\overline{\partial v}^*/\partial\phi)$ is negative between 20 and 45°N, and positive further north. The integral $C(K_{SE}, K_{TE})$ is hence a relatively small residue of two major contributions with opposite signs, and is therefore susceptible to large uncertainties.

- The estimates of $C(P_M, K_M)$ and $C(P_{SE}, K_{SE})$ are also quite different. Both terms are computed using the "V · grad Z" formulation described in PO, and so require an accurate determination of the ageostrophic flow. In view of the systematic bias of the wind data in the NMC set towards gradient wind balance over the data sparse regions, the correspond-

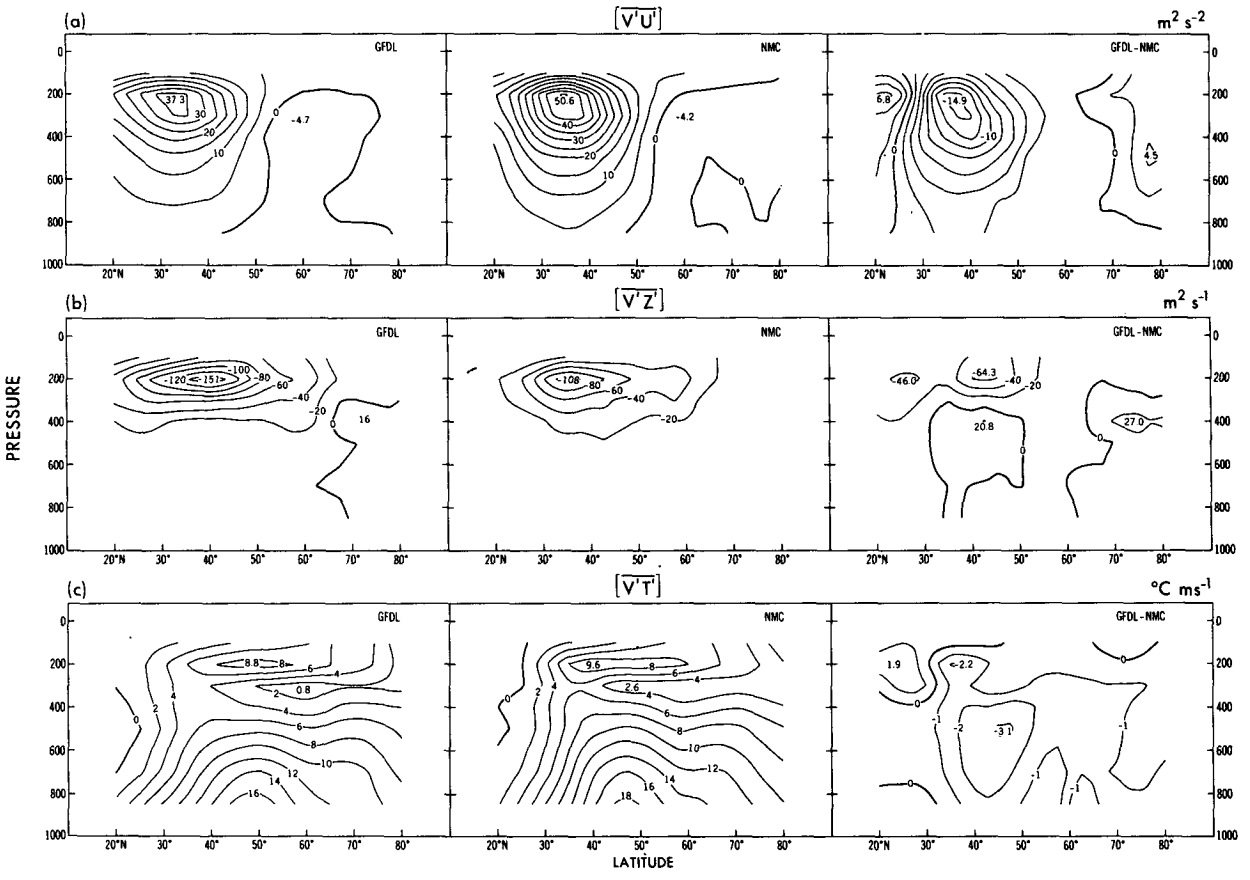

FIG. 12. As in Fig. 11, but for poleward transient eddy transport of (a) westerly momentum ($m^2\ s^{-2}$), (b) geopotential height ($m^2\ s^{-1}$), and (c) heat (°C $m\ s^{-1}$).

ing estimates of these terms are probably not realistic. The sign of the term $C(P_M, K_M)$ is governed by the relative contributions of the Hadley and Ferrel circulations within the domain considered. The disagreement between the two estimates of this term is apparently associated with the relatively weaker meridional circulations in the NMC set. Moreover, the poleward displacement of the Ferrel cell in the NMC pattern relative to its counterpart in the GFDL pattern tends to reduce the contribution of this thermally indirect circulation to the NMC estimate (see Fig. 13b in I).

It does not appear possible for the NMC estimates to fulfill the balance requirement for K_{SE}, since all processes (including dissipative friction) act to deplete energy from that reservoir (Fig. 13b).

• With the exception of $B(P_M)$ and $B(K_M)$, most of the boundary terms at 20°N play a relatively minor role in the energetics. The large discrepancies in the estimates of $B(P_M)$ and $B(K_M)$ result from the difference in the strength of the Hadley circulation at 20°N in the two sets (see Fig. 13b in I).

In Table 1, the estimates of various terms in the tropospheric energy cycle obtained here are compared with the corresponding values cited in a few earlier studies. In view of the voluminous works on atmospheric energetics during the past two decades, it is not feasible to include here a complete survey of the literature on this subject. We shall confine our attention to review articles of a comprehensive nature or to findings based on new data sets. These studies generally consider the tropospheric circulation over a substantial fraction of the Northern Hemisphere. Oort (1964) and Wiin-Nielsen (1964) reviewed the investigations prior to 1964, and presented energy flow diagrams by selecting the most representative estimates given by those studies. The observational studies of the energy cycle in the wavenumber domain were summarized by Saltzman (1970). A similar spectral formulation was used by Tomatsu (1979) to describe the energy budget on the basis of NMC analyses for 1964–65. Holopainen (1970) presented estimates of terms in the energy balance equation for the stationary waves. On the basis of a five-year collection of upper air soundings analyzed at GFDL, Peixóto and Oort (1974) and Oort and Peixóto (1974) presented the annual cycle of the atmospheric energetics. Rosen and Salstein (1980) compared the statistics derived from conventional station data and from NMC Hough analyses, and reported

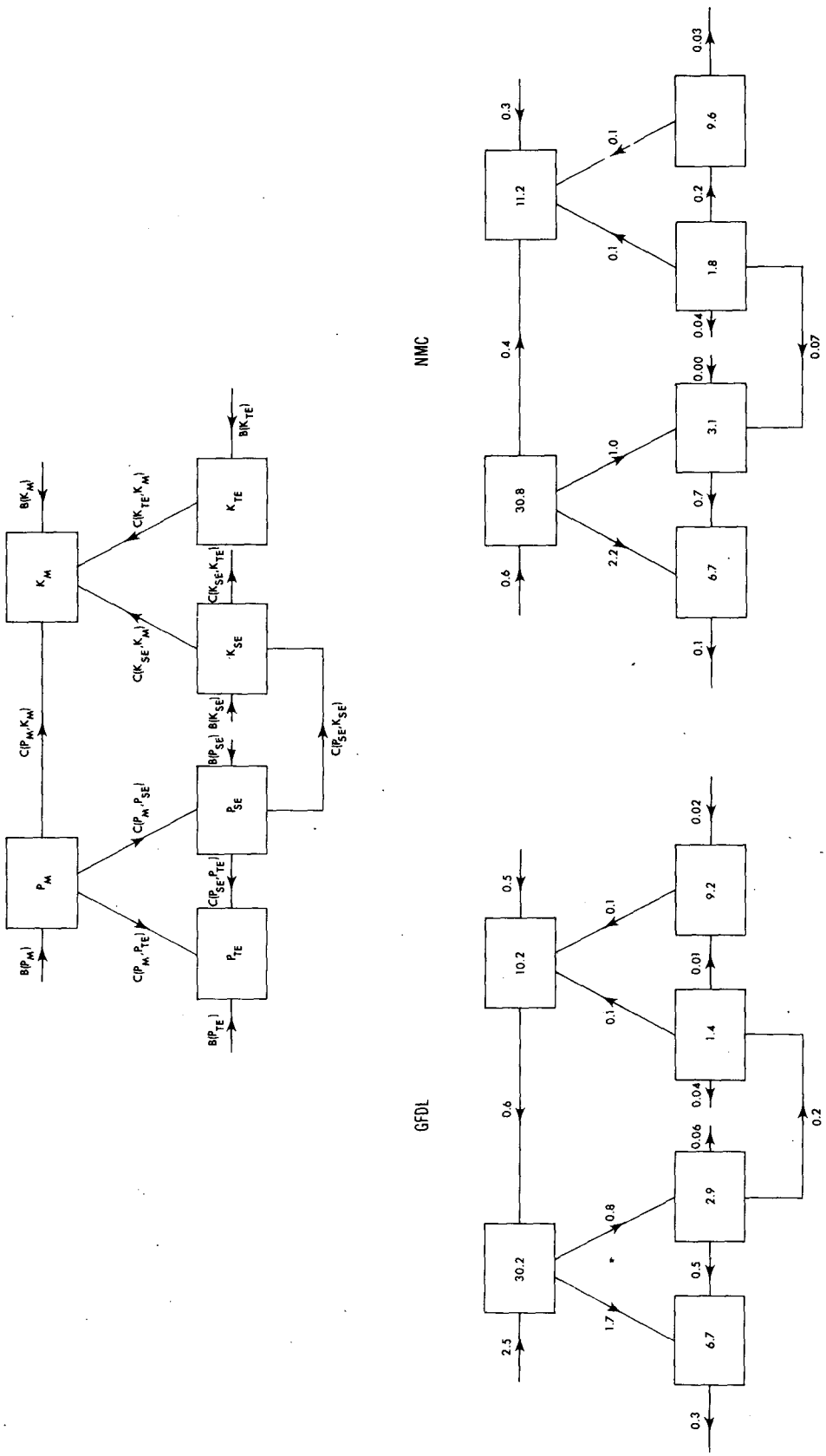

FIG. 13. Estimates of various components in the atmospheric energy cycle for the domain extending from 20 to 90°N and from 850 to 100 mb, based on (a) GFDL analysis and (b) NMC analysis for the winter season. Refer to the Appendix for definitions of symbols. Units for energy amounts, 10^5 J m^{-2}; for conversion rates, W m^{-2}.

TABLE 1. Estimates of various components of the energy cycle reported by selected investigators.[a]

	Oort (1964)		Wiin-Nielsen (1964)	Saltzman (1970)	Holopainen (1970)	Oort and Peixóto (1974) Peixóto and Oort (1974)	Tomatsu (1976)	Rosen and Salstein (1980)		This study	
	Annual mean		Winter	Winter	Winter	Jan '58–'63	Winter '64–'65	Winter '76–'77		Winter '66–'73	
	N Hemisphere		N Hemisphere 850–200 mb	20–87.5°N 1000–100 mb	15–90°N 1000–100 mb	N Hemisphere 1000–50 mb	25–75°N 925–100 mb	N Hemisphere 1000–50 mb		20–90°N 850–100 mb	
	Space domain	Space-time domain						Station data	NMC Data	GFDL Analysis	NMC Analysis
P_M	40	35	37.6	35.5		38[b]	22.5			30.2	30.8
K_M	8	5	13.6	10.0	8.5	8.0	8.9			10.2	11.2
P_E	15	20	10.7	11.2		16[b]	11.5			9.6	9.8
P_{SE}					7.1	4.6				2.9	3.1
P_{TE}						5.9				6.7	6.7
K_E	7	10	17.5	14.3	10.6	9.3	11.6			10.5	11.4
K_{SE}					1.5	2.1				1.4	1.8
K_{TE}					9.1	7.2				9.2	9.6
$C(P_M, K_M)$	0.1	−0.1	−0.2	0.0		−0.1	−0.6	0.2	0.0	−0.6	0.4
$C(P_M, P_E)$	3.0	1.5	3.8	5.3		2.8	4.6	2.7	2.8	2.5	3.2
$C(P_M, P_{SE})$					1.2	1.4		1.4	1.4	0.8	1.0
$C(P_M, P_{TE})$						1.4		1.3	1.4	1.7	2.2
$C(K_E, K_M)$	0.4	0.3	0.2	0.5		0.2	0.5	0.7	0.6	0.2	0.2
$C(K_{SE}, K_M)$					0.1			0.4	0.3	0.1	0.1
$C(K_{TE}, K_M)$								0.4	0.3	0.1	0.1
$C(P_{SE}, P_{TE})$					0.1					0.5	0.7
$C(K_{SE}, K_{TE})$					0.2					0.0 (0.0)[c]	0.2 (0.2)[c]

[a] Units for energy: 10^5 J m^{-2}; units for conversion rates: W m^{-2}; all conversion rates are rounded off to the nearest tenth of 1 W m^{-2}.
[b] Computed for the polar cap extending to 20°N.
[c] The values in parentheses are computed using the formulation of $C'(K_{SE}, K_{TE})$ given in Holopainen (1970). See Appendix for details.

energy conversion rates for the anomalous winter of 1976–77. The reader is referred to the above publications for detailed discussions of the computational procedures, and for a more complete bibliography of other related studies.

Keeping in mind that the estimates in Table 1 are influenced by the nonhomogeneities of the data base, budget formulation, and definition of the spatial and temporal domains in the above studies, the following remarks on these estimates can be made:

- The estimates on various forms of atmospheric energy are in reasonable agreement. The studies by Oort (1964), Holopainen (1970) and Wiin-Nielsen (1964) give relatively higher values for P_E, P_{SE} and K_E, respectively.
- Various studies yield conflicting estimates of the sign and magnitude of $C(P_M, K_M)$. In addition to the difficulties of obtaining reliable ageostrophic motions for the evaluation of this term, the result is also particularly dependent on the meridional extent of the integral, and on whether the "$\mathbf{V}\cdot\text{grad}Z$" or the "$\omega\alpha$" formulation is used (see PO).
- The use of the "space" domain (as opposed to the "mixed space-time" domain, see Oort, 1964) in the spectral studies of Saltzman (1970) and Tomatsu (1979) is probably a contributing factor to the relatively higher estimate of $C(P_M, P_E)$ and $C(K_E, K_M)$ they reported.
- The relatively higher estimate of $C(K_{SE}, K_M)$ reported by Rosen and Salstein (1980) for the winter of 1976–77 is probably a reflection of the highly amplified nature of the stationary waves during that winter.
- Due to constraints of data availability, Holopainen [1970, Eq. (25)] estimated the value of $C(P_{SE}, P_{TE})$ by correlating $\bar{T}^*$ at 500 mb with the divergence of the vertically integrated heat flux by transient eddies. Since the correlation between $\bar{T}^*$ and $\nabla\cdot\mathbf{F}(T)$ is strongest in the lower troposphere and decreases rapidly with height (Lau and Wallace, 1979, Figs. 3, 7 and 8), the approximation used in Holopainen's study tends to underestimate the magnitude of $C(P_{SE}, P_{TE})$. The corresponding estimates obtained in the present study are probably more realistic, since they are computed using statistics at individual pressure levels.

7. Summary

The present report enlarges the scope of an earlier comparative study of the GFDL and NMC analyses

by examining the temporal variance and covariance statistics. We have devoted a large part of the paper to a discussion of the similarities and differences in the spatial distributions of these statistics, because they are crucial to a better understanding of the interaction between the transient and stationary components of the atmospheric circulation. The findings reported here further demonstrate the impact of spatial data gaps and of the choice of the first-guess field on the final analyses in the two sets. Hence, most of the remarks in the introductory section of I also apply to the results in this part of the study. In particular, by using the 12 hour forecast field as the first-guess, the NMC synoptic analyses infer relatively stronger transient disturbances over the data-sparse oceans, which are known to be sites of enhanced eddy activities; whereas the use of the zonal mean as the first-guess in the same regions leads to relatively lower GFDL estimates for the eddy statistics. The influence of the first-guess field over the ocean basins is most evident in the maritime patterns of geopotential transport by the eddies (Fig. 9). Since the first-guess field for the NMC wind analyses is constrained to satisfy the gradient wind balance, the close correspondence between the vectors for $\mathbf{F}(z)$ and the $\overline{z'^2}$ contours [see Eq. (1)] in the NMC pattern (Fig. 9b) is ensured. The absence of such a dynamical constraint in the analysis procedure of the GFDL set results in a relatively weaker relationship between the $\mathbf{F}(z)$ and $\overline{z'^2}$ fields over the mid-oceans (Fig. 9a). On the other hand, the systematic bias of the NMC wind analyses towards gradient wind balance results in much weaker zonally averaged equatorward transports of geopotential energy (Fig. 12b), which depends on an accurate determination of the ageostrophic flow.

One striking feature which shows up in both sets of analyses is the tendency for the eddy heat flux vectors $\mathbf{F}(T)$ to be directed down the time-averaged local temperature gradient in the lower troposphere (Fig. 10). The transient eddies are hence very effective in dissipating the available potential energy of the stationary waves. The estimates of $C(P_{SE}, P_{TE})$ in this study are higher than those reported by Holopainen (1970) by an order of magnitude. The time scale associated with this dissipative mechanism, as given by the ratio $P_{SE}/C(P_{SE}, P_{TE})$, is approximately 6.7 (5.1) days for GFDL (NMC) analyses. Evaluation of the corresponding time scale in the kinetic energy balance, i.e., $K_{SE}/C(K_{SE}, K_{TE})$, is complicated by large uncertainties in the estimates of $C(K_{SE}, K_{TE})$, as has been noted in Section 6. The NMC analyses yield a dissipative time scale of approximately 10 days. The small value of $C(K_{SE}, K_{TE})$ based on GFDL analyses (Table 1) does not provide for a meaningful estimation of this time scale by the GFDL data set.

With the exception of $C(K_{SE}, K_{TE})$ and terms associated with the transformation of various forms of available potential energy [i.e., $C(P_M, K_M)$, $C(P_{SE}, K_{SE})$ and $C(P_{TE}, K_{TE})$], the differences between the GFDL and NMC estimates of most of the energy reservoirs and conversion rates in the energy cycle are <20% (Fig. 13). The systematic bias of the NMC wind analyses towards gradient wind balance over the data-sparse regions evidently precludes this set from yielding reliable estimates of the conversion terms connecting the available potential energy and kinetic energy reservoirs. Hence, the NMC estimates of these terms do not serve as meaningful checks of the corresponding values given by the GFDL set. The accuracy of the latter remains to be established by comparisons with other independent data sets containing realistic ageostrophic winds.

8. Epilogue

The earliest quantitative studies of the observed atmospheric circulation (e.g., Priestley, 1949; Starr and White, 1951) were conducted by compiling the required statistics at isolated stations. As the scope of the research programs expanded during the 1950's and 1960's, there was an increasing demand for a more comprehensive documentation of the spatial patterns of various circulation statistics, so that spatial integrals and local gradients could be more readily evaluated. A strategy, which seemed the most straightforward at that time for meeting these needs, was to construct analyzed charts based on the circulation statistics already accumulated at individual reporting stations (i.e., Scheme A as depicted in Fig. 2 of I). It was only later in the 1960's and 1970's, when numerical weather prediction became fully operational, that daily synoptic analyses could be used as an alternative data source for compiling circulation statistics (Scheme B in Fig. 2 of I).

To date, the most extensive compilations of circulation statistics based on Schemes A and B are probably the MIT/GFDL and NMC analyses examined here. For quite some time to come, it is anticipated that these statistics will serve as the data base for a large variety of observational studies on the general circulation. In undertaking this two-part comparative study, we have tried to discern those aspects of the observed general circulation which may be quantified by both sets of analyses with a reasonable degree of accuracy. Those circulation statistics, for which a close agreement between the estimates given by the GFDL and NMC analyses exist, would probably fall into this category. By the same token, we have also tried to identify those circulation features for which the two sets exhibit large differences. We bring these discrepancies to the attention of present and future users of these data sets in order to demonstrate that judicious use of the currently available observational data is in order, and that one needs to exercise caution while analyzing and inter-

preting those circulation statistics which are found to be subject to large uncertainties.

It is evident that the major obstacle to compiling reliable data sets with global coverage is the presence of spatial data gaps which are devoid of routine observations. To rectify this problem by installing more geographically-fixed rawinsonde stations and weather ships in the data-sparse regions seems economically infeasible. Considering that the primary data input for Scheme A is confined to statistics at fixed observing stations, and that purely statistical interpolation techniques do not introduce physical information into the data-sparse areas, future analyses based on Scheme A or its derivatives would be handicapped by the lack of real data input over the remote areas. However, the data source for Scheme A, i.e., the upper air soundings collected by the rawinsonde network, would remain a valuable compilation. By virtue of their "observational purity," these rawinsonde data provide the most reliable information available on the circulation at individual station sites. Hence, they should continue to fill the needs of various observational studies, particularly those which require temporally homogeneous records. Such station data also serve as useful "benchmarks" for comparison with the products of other future analysis schemes.

In recent years, the deployment of mobile observing platforms, such as weather satellites, aircraft, ships of opportunity, drifting buoys and balloons, collectively provide an unprecedented capacity for surveying the global circulation. At the same time, enormous efforts are being devoted to improve the performance of numerical models. We envision that the dynamical assimilation of the information collected by the modern sensing devices offers the best chance for determining circulation features over the oceans and other remote areas. Refined versions of Scheme B are the most likely candidates for accomplishing this objective in the near future. They are capable of utilizing a consistent dynamical framework to take full advantage of the information provided by both stationary and mobile platforms. In fact, the data handling procedures for the final data sets of the Global Weather Experiment are designed along the general principles behind Scheme B. However, intelligent strategies must be devised to avert the detrimental effects of constraints inherent in model initialization, balance procedures and physical parameterizations. In this respect, particular attention should be devoted to a reliable determination of the ageostrophic wind and vertical velocity fields.

Acknowledgments. We would like to thank Drs. E. O. Holopainen, J. D. Mahlman and S. Manabe for offering helpful comments on the manuscript. Dr. Glenn H. White kindly provided the NMC summertime statistics. Messrs. P. Tunison and his associates at GFDL drafted the figures. NCL is supported by NOAA Grant 04-7-022-44017.

APPENDIX

Formulation of the Energy Cycle

The formulation of the energy cycle in this study essentially follows that given in PO, except that the terms associated with eddies are partitioned into standing and transient components. The symbols used here have the same meaning as those in PO. In this study overbars are used to denote time averages.

The budget equations for various forms of energy can be expressed as:

$$\frac{\partial}{\partial t} P_M = G(P_M) - C(P_M, P_{SE}) - C(P_M, P_{TE}) - C(P_M, K_M) + B(P_M)$$

$$\frac{\partial}{\partial t} P_{SE} = G(P_{SE}) + C(P_M, P_{SE}) - C(P_{SE}, P_{TE}) - C(P_{SE}, K_{SE}) + B(P_{SE})$$

$$\frac{\partial}{\partial t} P_{TE} = G(P_{TE}) + C(P_M, P_{TE}) + C(P_{SE}, P_{TE}) - C(P_{TE}, K_{TE}) + B(P_{TE})$$

$$\frac{\partial}{\partial t} K_M = C(P_M, K_M) + C(K_{SE}, K_M) + C(K_{TE}, K_M) - D(K_M) + B(K_M)$$

$$\frac{\partial}{\partial t} K_{SE} = C(P_{SE}, K_{SE}) - C(K_{SE}, K_M) - C(K_{SE}, K_{TE}) - D(K_{SE}) + B(K_{SE})$$

$$\frac{\partial}{\partial t} K_{TE} = C(P_{TE}, K_{TE}) - C(K_{TE}, K_M) + C(K_{SE}, K_{TE}) - D(K_{TE}) + B(K_{TE}).$$

The definitions of P_M, P_{SE}, P_{TE}, K_M, K_{SE} and K_{TE} are given in PO [Eqs. (1)–(4)]. In this study all values are integrated between $p = 850$ and 100 mb, $\phi = 20$ and 90°N, $\lambda = 0$ and 360°.

a. Boundary terms

All boundary terms are evaluated at $\phi = 20$°N. $B(K_M)$ and $B(P_M)$ are defined in PO [Eqs. (10) and (12)].

$$B(K_{TE}) = \frac{1}{2}\int\int \overline{v(u'^2 + v'^2)}dxdp/g$$

$$B(P_{TE}) = \frac{C_P}{2}\int\int \gamma\overline{vT'^2}dxdp/g + \int\int \overline{v'\Phi'}dxdp/g$$

$$B(K_{SE}) = B(K_E) - B(K_{TE})$$

$$B(P_{SE}) = B(P_E) - B(P_{TE})$$

where $B(K_E)$ and $B(P_E)$ are defined in PO [Eqs. (9) and (11)].

b. Conversion terms

$C(P_{SE}, K_{SE})$, $C(P_{TE}, K_{TE})$ and $C(P_M, K_M)$ are defined in PO [Eqs. (14) and (15)]. $C(K_{SE}, K_M)$ and $C(K_{TE}, K_M)$ consist of those terms in PO [Eq. (13)] involving standing eddy statistics (i.e., those with asterisks) and transient eddy statistics (i.e., those with primes), respectively. $C(P_M, P_{SE})$ and $C(P_M, P_{TE})$ are those terms in PO [Eq. (16)] involving stationary eddy statistics and transient eddy statistics, respectively:

$$C(K_{SE}, K_{TE}) = -\int \left(\frac{\overline{u'u'}^*}{a\cos\phi}\frac{\partial \bar{u}^*}{\partial\lambda} + \frac{\overline{u'v'}^*}{a}\cos\phi\frac{\partial(\bar{u}^*/\cos\phi)}{\partial\phi} + \frac{\overline{u'v'}^*}{a\cos\phi}\frac{\partial\bar{v}^*}{\partial\lambda} + \frac{\overline{v'v'}^*}{a}\frac{\partial\bar{v}^*}{\partial\phi} - [\overline{u'u'}^*\bar{v}^*]\frac{\tan\phi}{a}\right)dm$$

$$C(P_{SE}, P_{TE}) = -C_P\int \gamma\left(\frac{\overline{u'T'}^*}{a\cos\phi}\frac{\partial\bar{T}^*}{\partial\lambda} + \frac{\overline{v'T'}^*}{a}\frac{\partial\bar{T}^*}{\partial\phi}\right)dm.$$

It should be noted that $C(K_{SE}, K_{TE})$ may be expressed as the sum of

$$C'(K_{SE}, K_{TE}) = \int \left\{\bar{u}^*\left(\frac{1}{a\cos\phi}\frac{\partial}{\partial\lambda}\overline{u'u'}^* + \frac{1}{a\cos^2\phi}\frac{\partial}{\partial\phi}\cos^2\phi\,\overline{u'v'}^*\right) + \bar{v}^*\left(\frac{1}{a\cos\phi}\frac{\partial}{\partial\lambda}\overline{u'v'}^* + \frac{1}{a\cos\phi}\frac{\partial}{\partial\phi}\cos\phi\,\overline{v'v'}^* + \frac{\overline{u'u'}^*}{a}\tan\phi\right)\right\}dm \quad \text{(A1)}$$

and the boundary term

$$\iint [\bar{u}^*\overline{u'v'}^* + \bar{v}^*\overline{v'v'}^*]dxdp/g. \quad \text{(A2)}$$

By incorporating (A2) into $B(K_{SE})$, the expression in (A1) may then be interpreted as an alternative form of the conversion rate from K_{SE} to K_{TE}, as was done in Holopainen [1970, Eq. (20)].

An analogous decomposition of $C(P_{SE}, P_{TE})$ may be performed. However, for both sets of analyses the estimate of the conversion rate between P_{SE} to P_{TE} is not sensitive to the particular formulation used.

c. Generation and dissipative terms

$D(K_M)$ and $G(P_M)$ are defined in PO [Eqs. (18) and (20)]. $D(K_{SE})$ and $D(K_{TE})$ are those terms in PO [Eq. (17)] involving stationary eddy statistics and transient eddy statistics, respectively. $G(P_{SE})$ and $G(P_{TE})$ are those terms in PO [Eq. (19)] involving stationary eddy statistics and transient eddy statistics, respectively.

The following terms cannot be evaluated directly in the present study:

1) Vertical advection through the 850 and 100 mb surfaces in the boundary terms.
2) Terms in $B(K_{TE})$ and $B(P_{TE})$ involving triple correlations in time.
3) Terms in the conversion rates involving vertical motions.
4) The conversion of available potential energy to kinetic energy in the transient eddies $C(P_{TE}, K_{TE})$.
5) The energy generation and dissipation terms $G(P_M)$, $G(P_{SE})$, $G(P_{TE})$, $D(K_M)$, $D(K_{SE})$ and $D(K_{TE})$.

REFERENCES

Holopainen, E. O., 1970: An observational study of the energy balance of the stationary disturbances in the atmosphere. *Quart. J. Roy. Meteor. Soc.*, **96**, 626–644.

Lau, N.-C., 1979: The observed structure of tropospheric stationary waves and the local balances of vorticity and heat. *J. Atmos. Sci.*, **36**, 996–1016.

——, and J. M. Wallace, 1979: On the distribution of horizontal transports by transient eddies in the Northern Hemisphere wintertime circulation. *J. Atmos. Sci.*, **36**, 1844–1861.

——, and A. H. Oort, 1981: A comparative study of observed Northern Hemisphere circulation statistics based on GFDL and NMC analyses. Part I: The time-mean fields. *Mon. Wea. Rev.*, **109**, 1380–1403.

——, G. H. White and R. L. Jenne, 1981: Circulation statistics for extratropical Northern Hemisphere based on NMC analyses. NCAR Tech. Note. TN-171 + STR, 138 pp.

Lorenz, E. N., 1955: Available potential energy and the maintenance of the general circulation. *Tellus*, **7**, 157–167.

Oort, A. H., 1964: On estimates of the atmospheric energy cycle. *Mon. Wea. Rev.*, **92**, 483–493.

——, 1982: *Global Atmospheric Circulation Statistics, 1958–1973.* NOAA Prof. Pap., in preparation.

——, and J. P. Peixóto, 1974: The annual cycle of energetics of the atmosphere on a planetary scale. *J. Geophys. Res.*, **79**, 2705–2719.

Peixóto, J. P., and A. H. Oort, 1974: The annual distribution of atmospheric energy on a planetary scale. *J. Geophys. Res.*, **79**, 2149–2159.

Priestley, C. H. B., 1949: Heat transport and zonal stress between latitudes. *Quart. J. Roy. Meteor. Soc.*, **75**, 28–40.

Rosen, R. D., and D. A. Salstein, 1980: A comparison between circulation statistics computed from conventional data and NMC Hough analyses. *Mon. Wea. Rev.*, **108**, 1226–1247.

Saltzman, B., 1970: Large-scale atmospheric energetics in the wave-number domain. *Rev. Geophys. Space Phys.*, **8**, 289–302.

Starr, V. P., and R. M. White, 1951: A hemispherical study of the atmospheric angular momentum balance. *Quart. J. Roy. Meteor. Soc.*, **77**, 215–225.

Tomatsu, K., 1979: Spectral energetics of the troposphere and lower stratosphere. *Advances in Geophysics*, Vol. 21, Academic Press, 289–405.

Wiin-Nielsen, A., 1964: Some new observational studies of energy and energy transformations in the atmosphere. WMO Tech. Note 66, 177–202.